SPREAD: a simplified tool for the nose-to-tail analysis of an airbreathing hypersonic vehicle

Filomena Piscitelli, Luigi Cutrone, Giuseppe Pezzella, Pietro Roncioni, Marco Marini
CIRA, Italian Aerospace Research Centre
Via Maiorise, 81043 Capua (CE), Italy

Abstract

SPREAD (Scramjet PREliminary Aerothermodynamic Design) code is an in-house simplified design tool developed by CIRA (Italian Aerospace Research Centre), which allows a real-time screening of several engine/aircraft configurations and the identification of the most promising one/s with respect to user-defined constraints and requirements. The outcome of this procedure defines the base-line for further design analyses with more accurate tools. The present research effort reports on the application of SPREAD tool to the nose-to-tail analysis of the LAPCAT-II Mach 8 MR2.4 vehicle configuration. Numerical results demonstrate SPREAD capability to quickly predict reliable values of aero-propulsive balance (i.e., net-thrust) and aerodynamic efficiency in a pre-design phase.

Nomenclature

Latins

AoA	angle-of-attack [deg]
APB	aero-propulsive balance [kN]
C_D	drag coefficient
C_f	skin-friction coefficient
C_p	pressure coefficient
CFD	Computational Fluid Dynamics
D	drag force [kN]
EINO	Emission Index NO [g_{NO}/kg_{fuel}]
E.R.	effective fuel-air equivalence ratio
L	lift force [kN]
M	Mach number
P	pressure [Pa]
S	surface [m^2]
SA0	Spalart-Allmaras standard turbulence modelling
T	temperature [K], thrust force [kN]
TURB	turbulent flow
X,Y,Z	spatial coordinates [m]

Greeks

Δ	variation
η	efficiency

Subscripts

cc	combustion chamber
comb	combustion related
ext	external
friction	friction related
fuel	fuel related
H_2	hydrogen related
int	internal
prop	propulsive
ref	reference
wet	wetted
∞	free stream conditions

1. Introduction

In the last years there has been a growing worldwide interest on hypersonic airbreathing vehicles [1] aiming to reduce both the cost of space access (Single Stage To Orbit vehicle) and the travelling time of antipodal civil flights (e.g., Brussels to Sydney in 3÷4 hours). For a hypersonic vehicle, the separation between the engine and the aircraft, typical of conventional subsonic and supersonic configurations is less evident and the achievement of the best integration between airframe and propulsion system is a strong design constraint. Indeed, as shown in Figure 1, the whole lower surface of the forebody can be used as an intake for flow compression, i.e., the oncoming airflow is compressed by means of oblique shock waves generated by the vehicle forebody, thus avoiding the use of compressors and turbines. Such an absence allows these engines to reach higher temperatures at the end of the combustor and, as a consequence, higher thermal efficiencies and larger thrust-to-weight ratios. On the other hand, the burned gases exiting the combustor can expand along the internal nozzle and entire afterbody, this latter acting as an additional expansion nozzle.

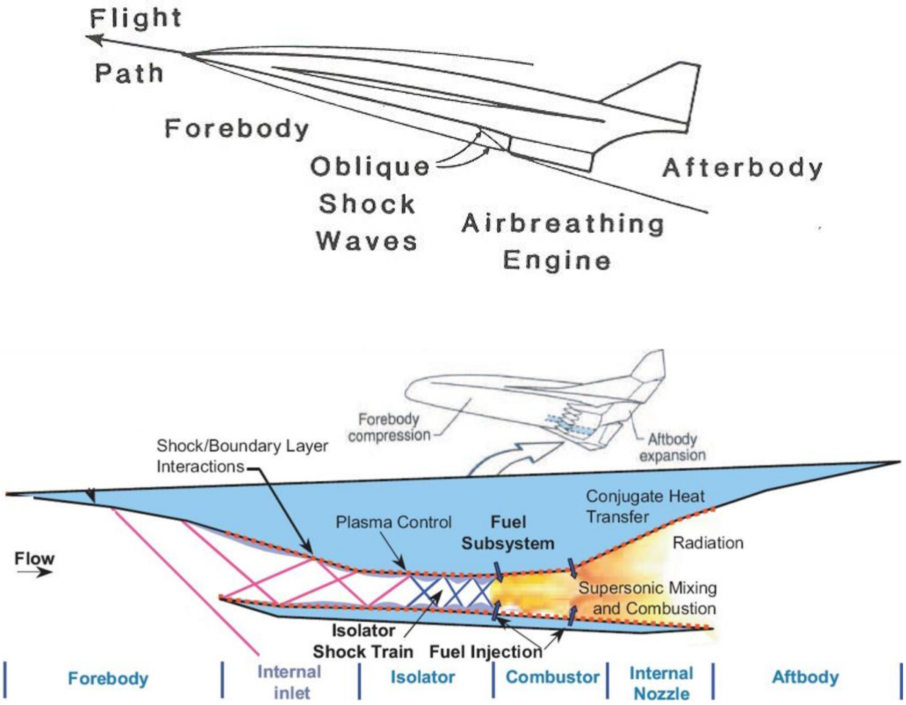

Figure 1: Schematic view of a hypersonic air-breathing engine vehicle with full airframe-propulsive system integration.

Due to the strong coupling between the aerothermodynamic (external) and propulsive (internal) flow fields, an accurate prediction of the engine's performances can only be attained by means of CFD simulations and wind tunnel testing of the integrated configuration. Nevertheless, less expensive and time-consuming methods can provide a useful support to the preliminary analysis and design of the vehicle's configuration and its propulsive system.

In this scenario, the SPREAD (Scramjet PREliminary Aerothermodynamic Design) code developed by the Italian Aerospace Research Centre allows for a real-time simplified design and analysis of several engine/airframe configurations and the identification of the most promising one/s with respect to user-defined constraints and requirements. The code consists of two modules for design and analysis purposes: an engine module [2],[3] and an aerothermodynamic module [4], whose mathematical formulation is not here reported for the sake of brevity. The outcome of this code defines the baseline configuration of the vehicle for further analyses with more accurate tools. The present research reports on the application of SPREAD tool to the nose-to-tail analysis of the LAPCAT-II Mach 8 MR2.4 vehicle configuration (Figure 2) in hypersonic flight conditions [5],[6],[7].

Figure 2: MR2.4 vehicle by ESA-ESTEC.

Both external aerothermodynamics and internal engine's flow have been analysed, and high speed aerodynamic parameters (lift, drag, aerodynamic efficiency) and engine performance parameters (thrust, combustion efficiency, emissions) have been evaluated.

2. The MR2.4 vehicle in hypersonic flight conditions

The LAPCAT-II MR2.4 vehicle developed by ESA-ESTEC (see a pictorial view in Figure 2) is a winged waverider designed to fly at Mach 8, equipped with a dorsal mounted dual-mode ramjet (DMR) engine fuelled by hydrogen, and accelerated by a number of turbojet engines based on an air-turbo rocket (ATR) cycle up to Mach 4.5 (switching from ATR to DMR) [8]. The vehicle is characterised by an elliptical intake with aspect ratio of 3, a geometrical contraction ratio of 7.8, a constant cross-section combustion chamber and a two-sector expansion nozzle with an overall expansion ratio of 22.1. Planned maximum take-off weight (MTOW) is 400 tons, while main dimensions (length, span) are reported in Figure 3.

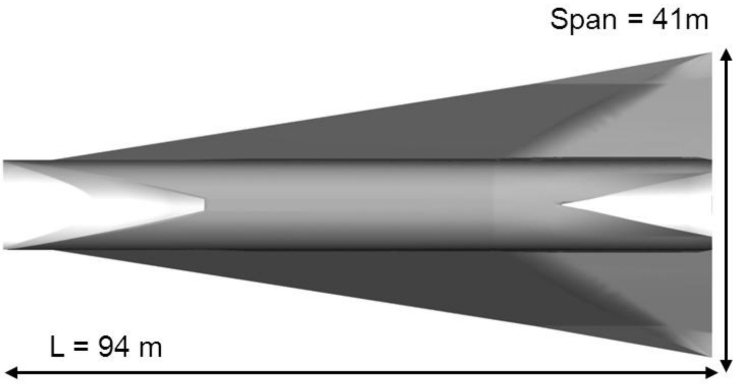

Figure 3: MR2.4 vehicle main dimensions.

The mission profile foresees an antipodal flight (i.e., from Brussels to Sidney, range 16200 km) carrying 300 passengers with an efficient cruise at an altitude of about 30÷35 km. The flight time is nearly 3 hours. The cruise scramjet mode operates for nearly 12000 km and for 80 minutes at an altitude varying from about 31 to 35 km. Then there is the scramjet engine switch off, the gliding for 2000 km and finally the landing. The MR2.4 schematic flight trajectory is reported in Figure 4.

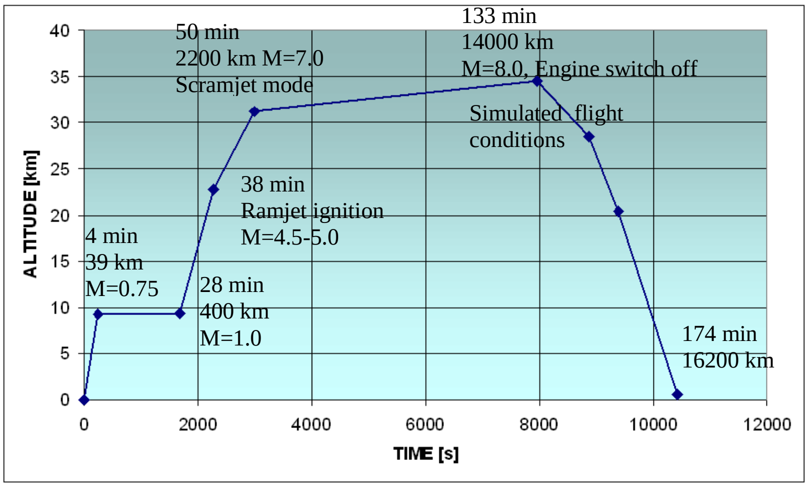

Figure 4: MR2.4 preliminary trajectory.

A view of the internal scramjet flowpath is shown in Figure 5 as half configuration: the elliptical intake, the constant cross section (S_{cc}=4.9 m^2) combustion chamber, and the two-sector expansion nozzle.

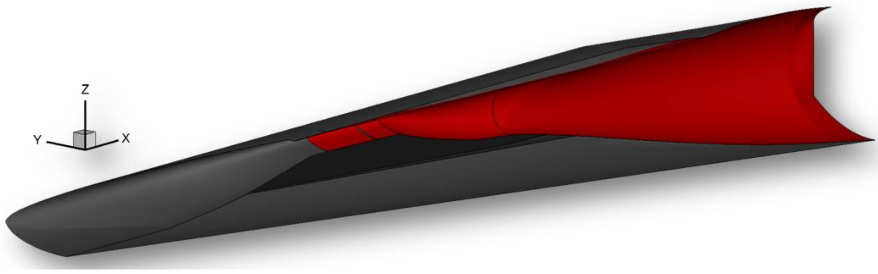

Figure 5: MR2.4 propulsive internal flowpath (half configuration).

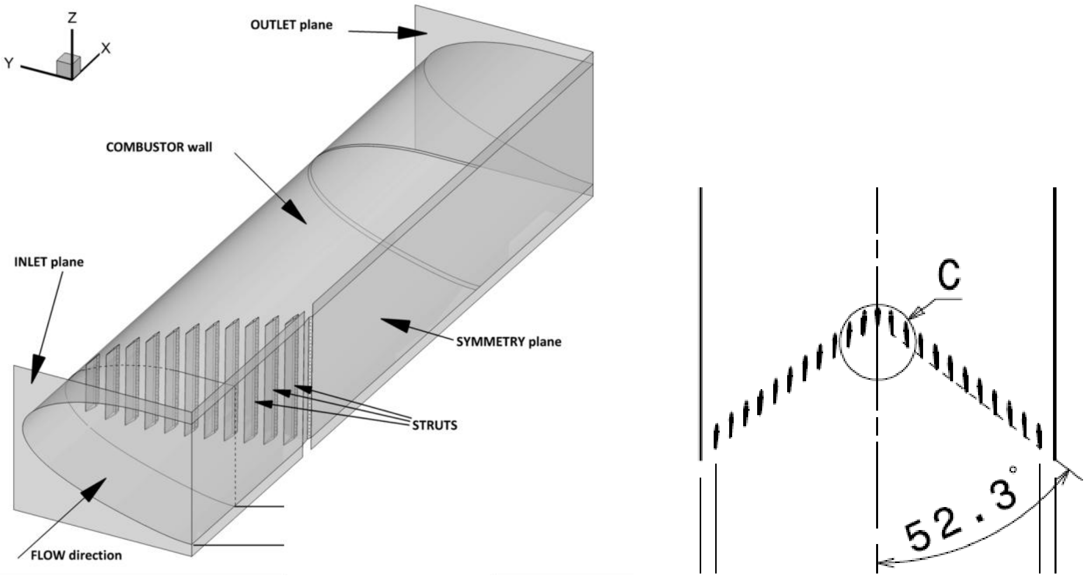

Figure 6: MR2.4 scramjet combustion chamber (half configuration) and struts layout.

Details of the combustion chamber are shown in Figure 6, where the 8.3m long chamber is reported with the 23 struts (1248 fuel injection port-holes) mounted in a V-shape layout (Figure 6, right) for a 1.5m length of the injector set. The hypersonic flight condition considered for the present nose-to-tail analysis of the MR2.4 configuration, to be compared with CFD results of [8] and [9], is fully reported in Table 1.

Table 1: Hypersonic flight condition of the nose-to-tail analysis of the MR2.4 configuration.

Mach	Altitude [km]	AoA. [deg]	P_∞ [Pa]	T_∞[K]	E.R.	T_{H2} [K]
8	31.95	0	896.09	228.46	0, 0.6	500

3. The internal scramjet flowpath

After the development, demonstration and validation of the SPREAD engine module [2],[3], the tool has been applied to the MR2.4 vehicle configuration in hypersonic flight conditions of Table 1. An inviscid analysis of the overall engine with a H_2/air combustor having a variable section area has been performed. Equivalence ratio is E.R.=0.6 and injection temperature of hydrogen is 500 K.

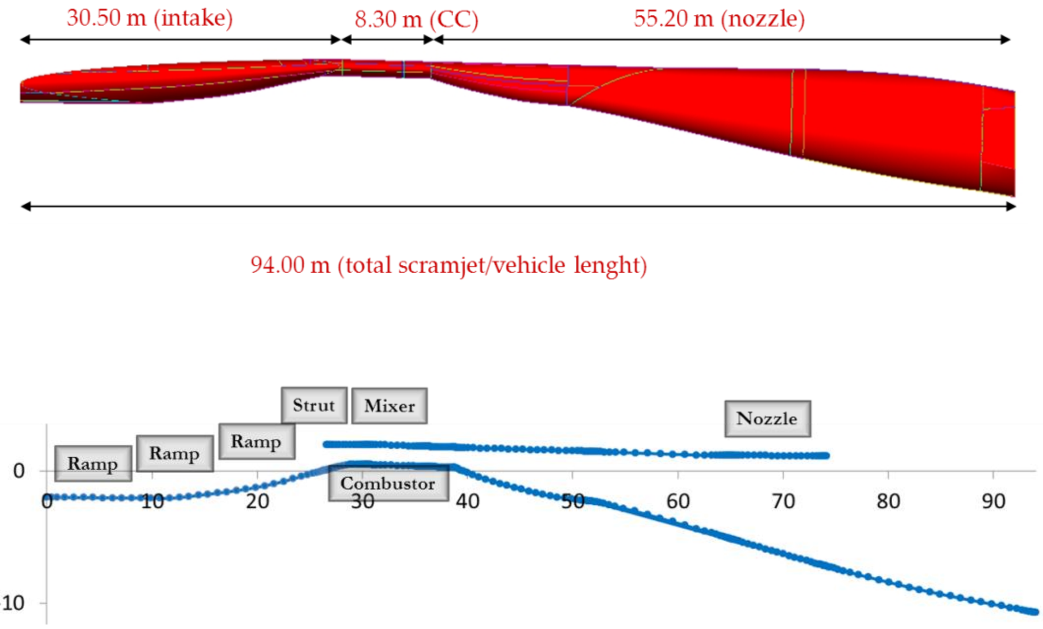

Figure 7: Scramjet propulsion flowpath (top) and SPREAD schematization (bottom).

The entire scramjet engine flowpath is shown in Figure 7, as well as its SPREAD schematization: a 3-ramp intake followed by an equivalent combustor at constant width and rectangular section, and by the two-sector expansion nozzle. It must be highlighted that ΔP and ΔT generated by the presence of struts (see Figure 6) are extracted by the combustion chamber CFD simulations [8],[9] and imposed at the injection section (i.e., the "strut" box) in order to have the proper ignition of air-hydrogen mixture. The accuracy of SPREAD predictions has been verified by comparing the 1-D results with those of the CFD simulation (section averaged distributions) performed by means of the CIRA SPARK CFD code, [8],[9], for the full vehicle configuration (with 1D/3D combustion coupling). Figure 8 shows the pressure and temperature distributions along the scramjet engine, whereas Figure 9 reports the water mass fraction, i.e., a product of combustion. Results highlight a globally good and satisfactory agreement of SPREAD predictions with CFD results, also considering that in the SPREAD simulation air and hydrogen are assumed completely mixed at the position of the last strut in the combustor center-plane.

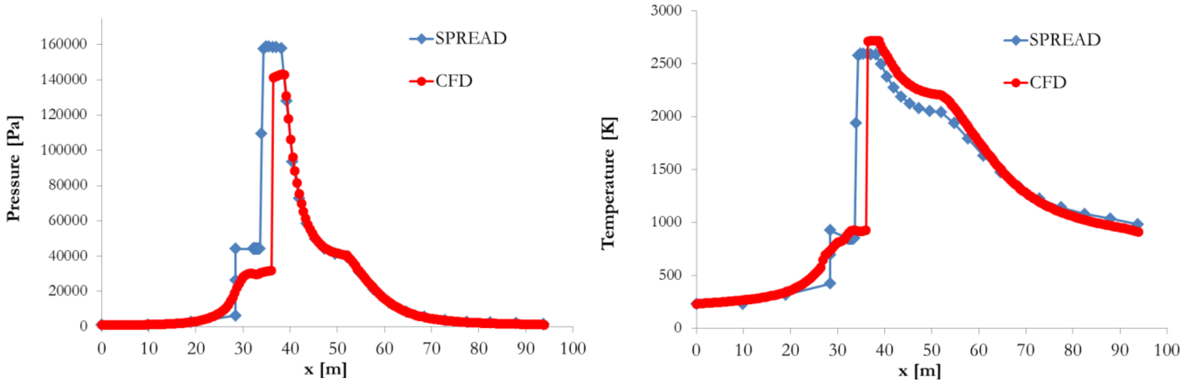

Figure 8: Pressure (left) and temperature (right) evolution along the scramjet engine.

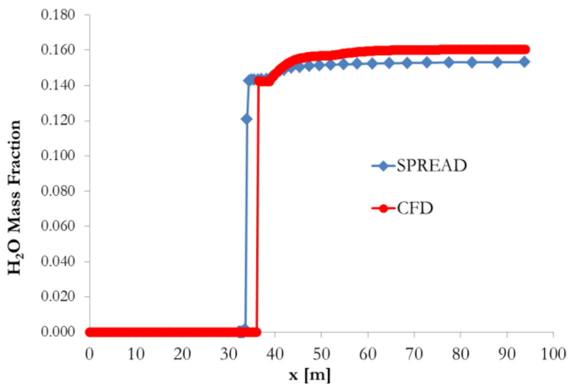

Figure 9: Water mass fraction evolution along the scramjet engine.

In addition, a more accurate comparison has been made between SPREAD 1-D predictions along the combustion chamber and the results of the full combustor 3D simulation performed by CIRA with an unstructured grid of about 11-million cells [8],[9]. The comparison, in terms of combustion efficiency along the combustor shown in Figure 10, highlights a clearly delayed combustion predicted by SPREAD which can be easily explained by differences in injector's modelling: nevertheless, the final value of combustion efficiency is in perfect agreement with SPARK. For what concerns the ignition delay, and consequently the dimensioning of the combustor, SPREAD prediction can be considered "conservative". The ignition delay observed in the SPREAD result is also the cause of a delayed NO_x release, as shown in Figure 11 in terms of emission index. Even though the slope of the EINO release curve is similar between SPREAD and SPARK, and the SPREAD result agrees quite well with SPARK result, as long as the ignition point is properly shifted, in this case SPREAD prediction of the final level of NO emissions produced by the scramjet combustor is "too optimistic".

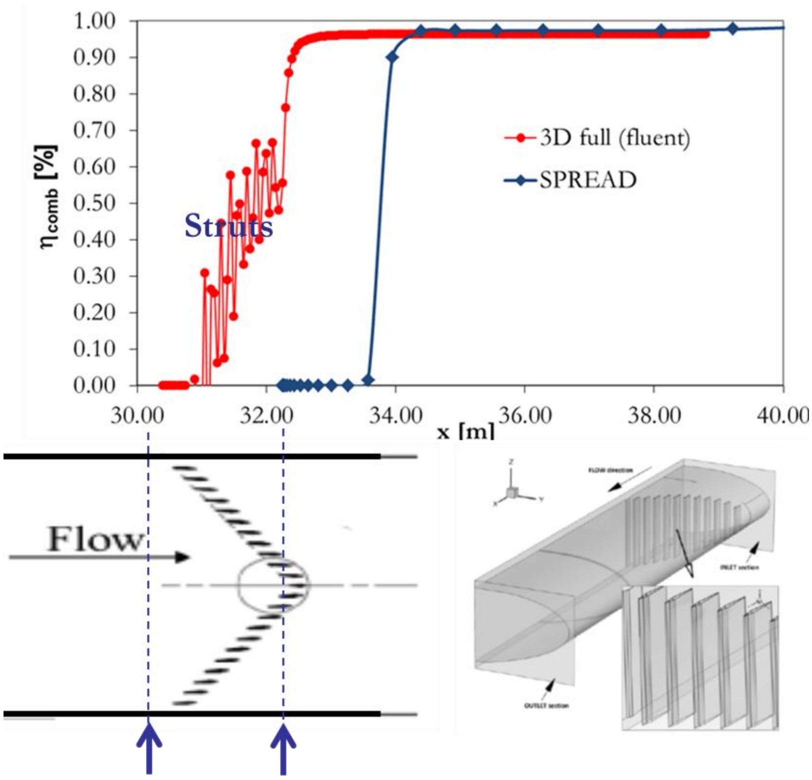

Figure 10: Combustion efficiency evolution along the scramjet combustor.

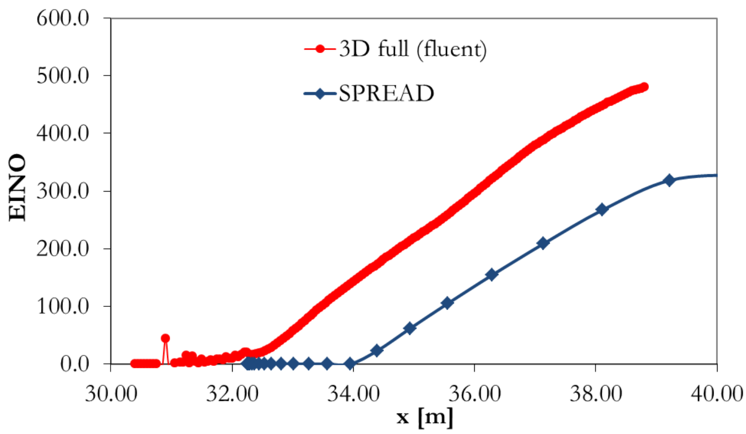

Figure 11: EINO evolution along the scramjet combustor.

4. The external aerothermodynamic field

A 3D Supersonic-Hypersonic Panel Method based on surface inclination methods including viscous effects, developed and validated in [4] and [10], has been applied to the MR2.4 vehicle configuration for a quick prediction of the aerodynamic performance at the hypersonic flight conditions of Table 1. Vehicle surface is approximated with a system of planar panels, and the surface mesh necessary to the aerothermodynamic module of SPREAD code to perform the engineering aerodynamic and aerothermodynamic analysis has been generated by means of ANSYS-ICEMCFD® commercial software package, see Figure 12 [10].

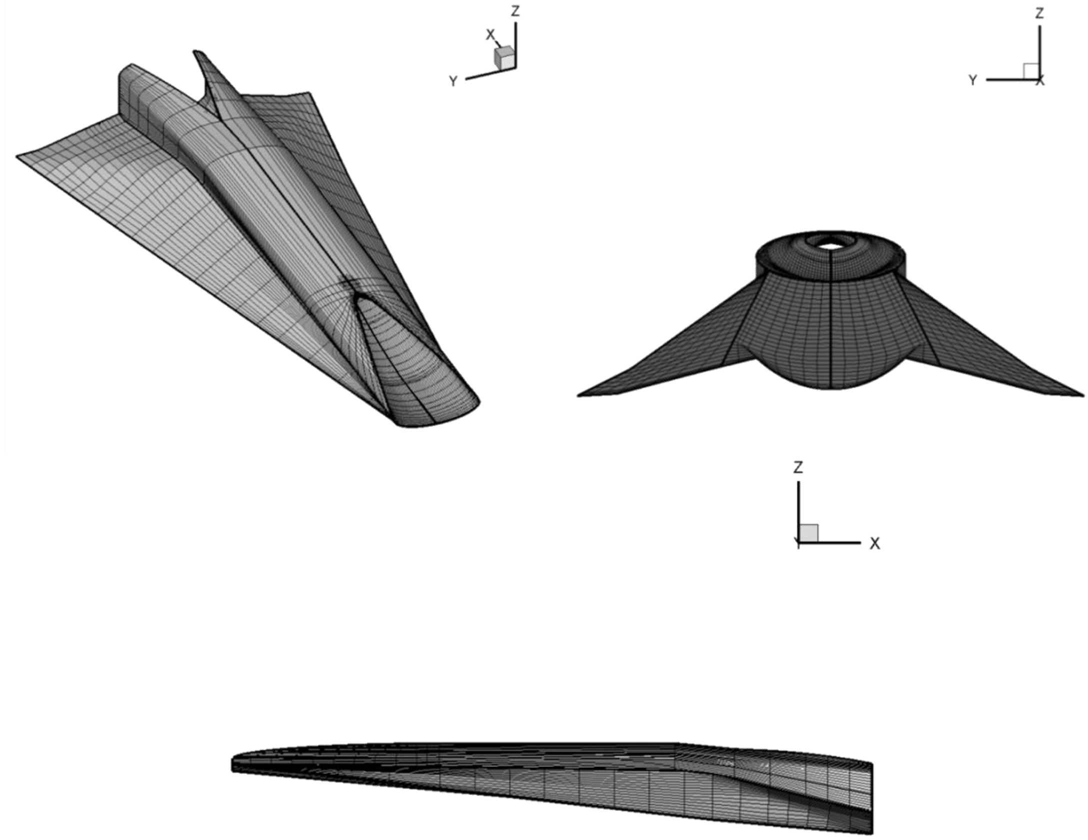

Figure 12: MR2.4 vehicle external surface mesh (3 views).

The pressure acting on each panel, in impact and shadow regions, is evaluated by user-specified compressor-expansion theory. Several methods and theories [11],[12] are available in the aerothermodynamic module of SPREAD and are reported below.

Impact flow	Shadow flow
Modified Newtonian	Newtonian
Modified Newtonian/ Prandtl-Meyer	Modified Newtonian/ Prandtl-Meyer
Tangent wedge	Prandtl-Meyer empirical
Tangent wedge empirical	OSU blunt body empirical
Tangent cone empirical	Van Dyke unified method
OSU blunt body	High Mach no. base pressure
Van Dyke unified method	Shock expansion method
Blunt body skin friction	Input pressure coefficient
Shock expansion method	Free molecular flow
Free molecular flow	
Input pressure coefficient	
Hankey flat surface empirical	
Delta wing empirical	
Dahlem-Buck empirical	
Blast wave	
Modified tangent code	

For instance, the tangent-wedge empirical method has been considered for the vehicle’s windside (e.g., both for wings and fuselage), while for the MR2.4 leeside Newtonian and Prandtl-Meyer theories have been applied for fuselage and wings, respectively. Fully turbulent viscous effects have been taken into account through approximate boundary layer methods for the external vehicle’s surfaces. As far as the viscous contribution to aerodynamic forces and moments is concerned, it is worth noting that the shear force is determined on each vehicle panel, considered as a flat plate. In particular, the skin friction for laminar or turbulent flat plate is assumed to be equal to:

$$\Delta C_{D,friction} = c_f \frac{S_{wet}}{S_{ref}}$$

where C_f is the skin friction coefficient, S_{wet} is the panel wetted area and S_{ref} is the vehicle's reference surface [12]. Reference temperature and reference enthalpy methods are available for both laminar and turbulent flows. The viscous calculation is performed along streamlines, and the results are then interpolated to the panel centroids. The streamlines have been traced on the configuration, described by quadrilateral elements, by using the Newtonian steepest descent method, which uses only the element inclination angle relative to the velocity vector to determine the streamline trace [4]. Global vehicle aerothermodynamic coefficients have been obtained by appropriate summation of the contributions of each component, following the well-known build-up approach [4],[13]. Some results of MR2.4 external aerodynamics are shown in the following figures, where computed pressure coefficient contours for M_∞=8 and AoA=0 deg are shown.

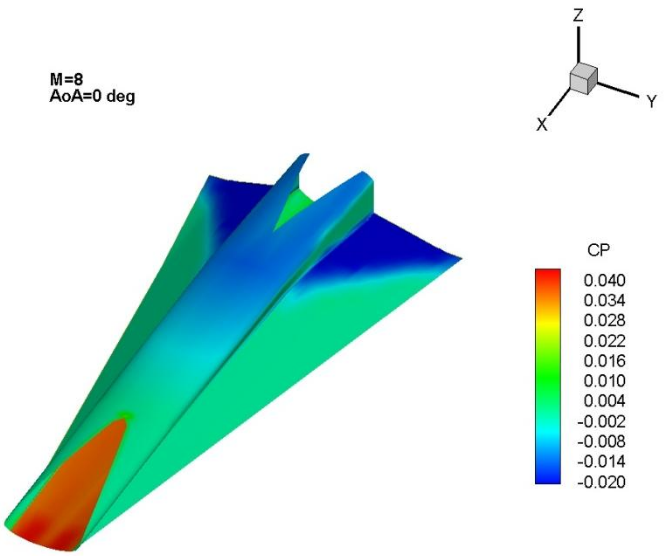

Figure 13: MR2.4 vehicle surface pressure coefficient contours, leeside.

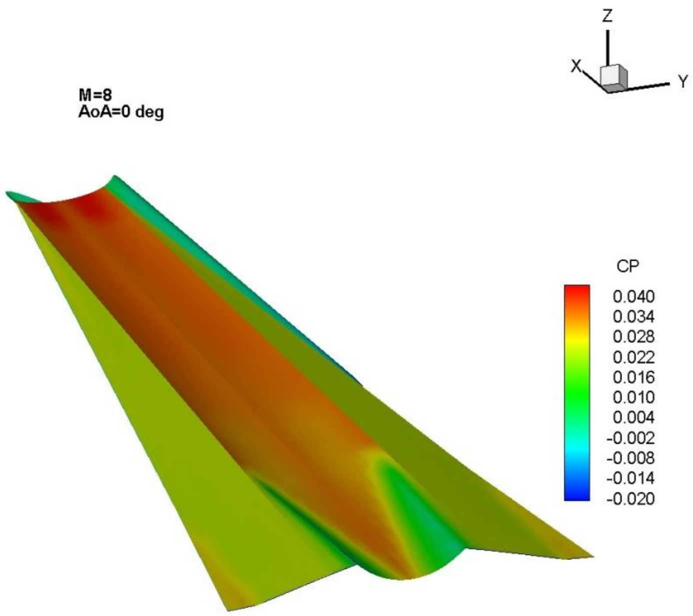

Figure 14: MR2.4 vehicle surface pressure coefficient contours, bottom windside.

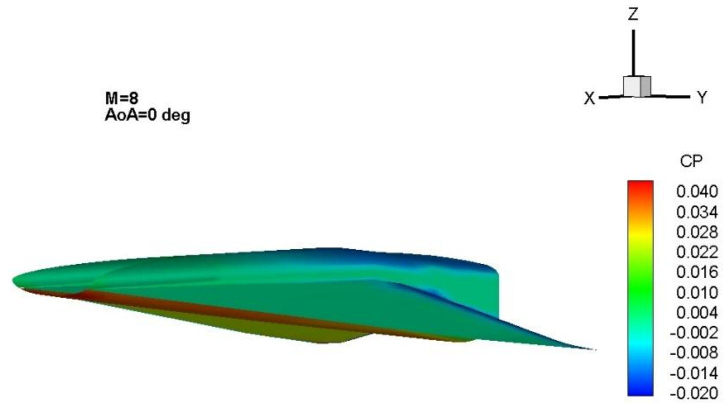

Figure 15: MR2.4 vehicle pressure coefficient contours, lateral view.

The SPREAD aerothermodynamic module results clearly show the presence of strong flow expansions on the rear leeside part of the wings (see Figure 13), the compression on vehicle windside followed by some expansions on the rear sides of the fuselage (see Figure 14), as well as the effect of the shape of wing tips (Figure 15).
The accuracy of the SPREAD external aerodynamic predictions has been verified by comparing these results with those of the CFD simulations performed by means of the CIRA SPARK code, [8],[9], in particular with the fully turbulent CFD solution obtained by using the Spalart-Allmaras standard turbulence modeling (TURB SA0).

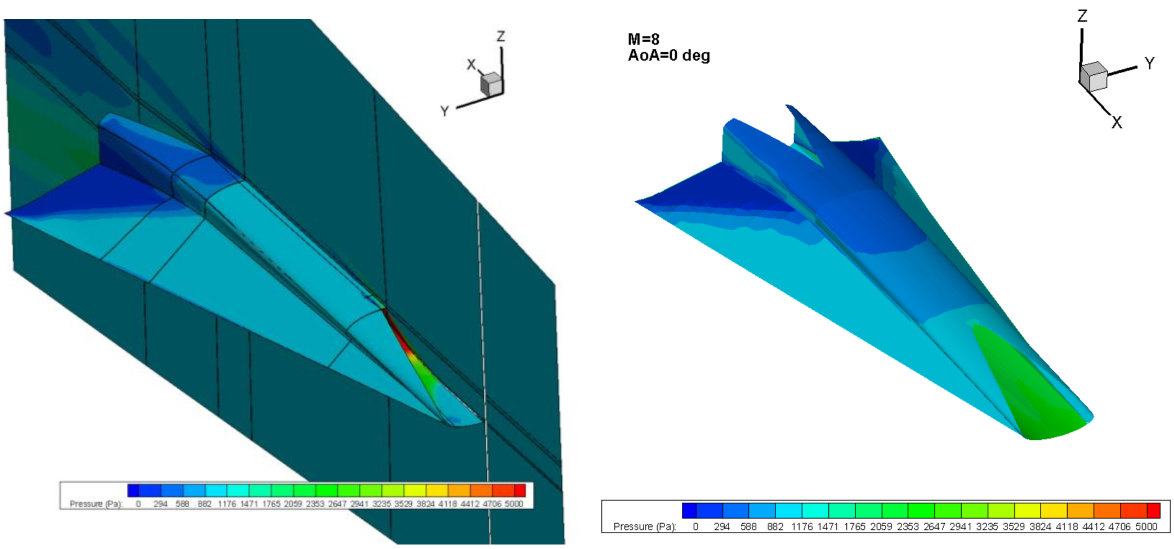

Figure 16: MR2.4 vehicle pressure contours, CFD TURB SA0 (left) and SPREAD (right).

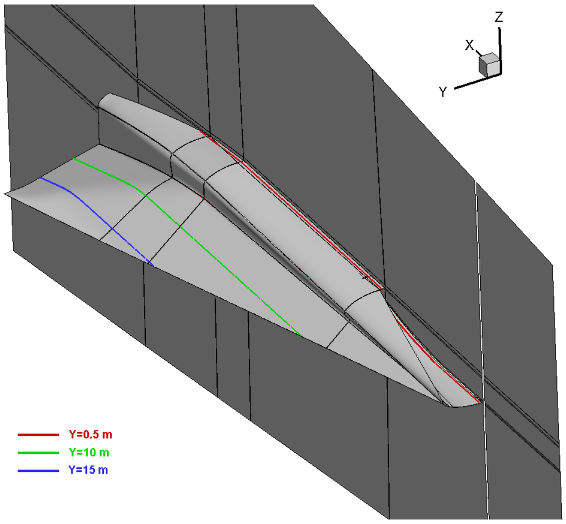

Figure 17: MR2.4 vehicle longitudinal sections (Y=0.5, 10, 15 m).

Figure 16 shows the comparison between CFD and SPREAD predictions in terms of pressure contours on the external surfaces of the vehicle, while Figure 17 shows three longitudinal sections at different span (Y=0.5, 10, 15 m) where pressure coefficient distributions have been extracted and compared, see Figure 18 and Figure 19.

The agreement is satisfactory in terms of pressure coefficient distributions, in particular along with the fuselage windside and leeside (see Figure 18) and along with the wing leeside at both spans (see Figure 19), where the local expansion due to wing shape is perfectly predicted. On the contrary, some discrepancies appear in the wing windside, mainly because SPREAD is not able to capture the hypersonic viscous interaction phenomenon occurring at the wing leading edge (due to the simultaneous presence of a growing boundary layer and an oblique shock wave).

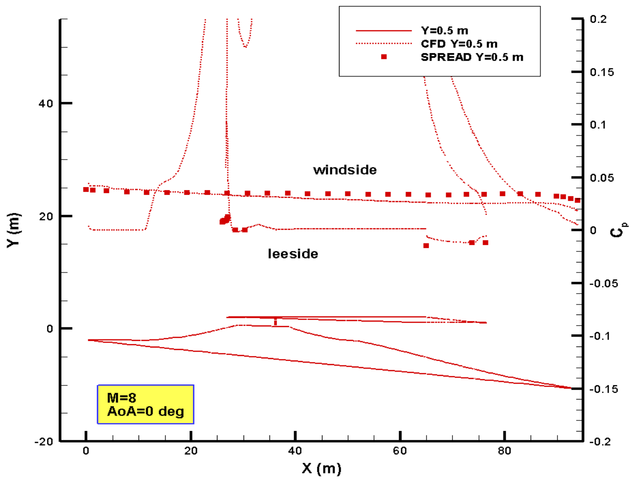

Figure 18: MR2.4 vehicle longitudinal C_p distribution at section Y=0.5 m.

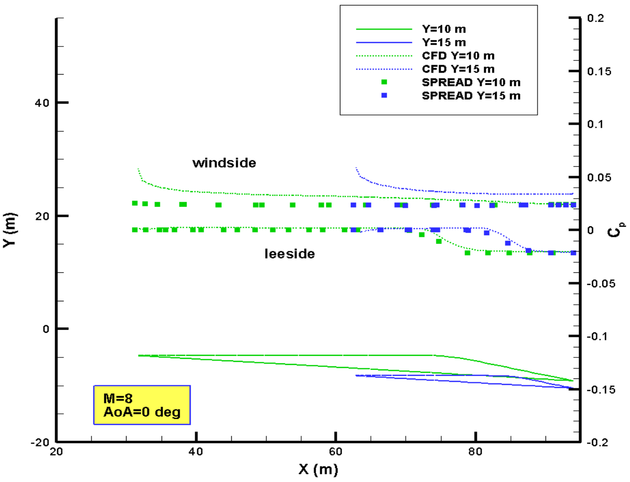

Figure 19: MR2.4 vehicle longitudinal C_p distribution at sections Y=10, 15 m.

5. Coupled nose-to-tail analysis and discussion of results

The final aero-propulsive performance of the MR2.4 vehicle in hypersonic flight conditions has been predicted by a coupled nose-to-tail analysis, and SPREAD results have been compared to CFD results, in both fuel-off (E.R.=0) and fuel-on (E.R.=1) conditions. A weak coupling of the two modules of SPREAD tool, the engine one (ENG) and the aerothermodynamic (ATD) one, has been realized by interpolating the section-averaged data predicted by the engine module onto the surface mesh built for the internal flowpath. Then, the forces and moments (following the build-up approach) have been assessed by using the aerothermodynamic module, whereas the internal flowpath, accounted as an additional component contributing to forces and moments as well, has been extracted by the engine module. Fully turbulent viscous effects have been taken into account for the external vehicle's surfaces by means of proper boundary layer corrections, whereas for the internal flowpath viscous turbulent corrections have been derived from CFD data [8],[9]. The results of the nose-to-tail analysis of the MR2.4 vehicle are reported in Table 2 and Table 3, in terms of global aerodynamic coefficients, aero-propulsive balance and aerodynamic efficiency (L/D_{ext}). SPREAD predictions have been compared to available CFD results from CIRA and ESA-ESTEC, [8],[9].
The following equation has been considered for the aero-propulsive balance (i.e., the net-thrust):

$$APB = D_{ext} + D_{int} = D_{ext} - T_{prop}$$

where the propulsive thrust T_{prop} is equal and opposite to the internal drag D_{int}, i.e. the sum of the drag of intake, combustion chamber and nozzle.

Table 2: MR2.4 vehicle global aerodynamic coefficients.

Simulation	Comb. Coupling	Partner	E.R.	L [kN]	D_{ext} [kN]	D_{int} [kN]	D_{pres} [kN]	D_{visc} [kN]
CFD TURB SA0	1D/3D	ESTEC	0	3453.00	467.00	176.00	337.00	306.00
SPREAD	**ATD**	**CIRA**	**0**	**3095.97**	**409.63**	**254.77**	**373.26**	**291.14**
CFD TURB SA0	1D/3D	CIRA	0.6	3372.30	511.20	-467.20	-364.00	408.00
CFD TURB SA0	3D/3D	CIRA	0.6	3438.00	534.00	-339.00	-251.00	446.00
SPREAD	**ATD+ENG**	**CIRA**	**0.6**	**2971.92**	**525.25**	**-381.53**	**-179.44**	**323.16**

Table 3: MR2.4 vehicle aero-propulsive balance and aerodynamic efficiency.

Simulation	Comb. Coupling	Partner	E.R.	APB [kN]	(L/D_{ext})
CFD TURB SA0	1D/3D	ESA	0	643.00	7.39
SPREAD	**ATD**	**CIRA**	**0**	**664.40**	**7.56**
CFD TURB SA0	1D/3D	CIRA	0.6	44.00	6.60
CFD TURB SA0	3D/3D	CIRA	0.6	195.00	6.44
SPREAD	**ATD+ENG**	**CIRA**	**0.6**	**143.72**	**5.66**

Apart from the general good prediction (with respect to CFD results) of external aerodynamics and engine’s internal flowpath, as shown in the previous sections, from the coupled nose-to-tail analysis it can be observed and summarized that for fuel-off conditions, APB and L/D_{ext} are well predicted by SPREAD, whilst lift is underestimated of about 10%. Additionally, for fuel-on conditions, the agreement of results depends upon the combustion coupling method: SPREAD fuel-on solution is closer to 3D/3D (combustion coupling) CFD solution [9], and this is because ΔP and ΔT caused by struts and viscous corrections have been taken by that CFD solution (further developments should include tools able to predict local increases of pressure and temperature due to the presence of struts). Lift is still ~10% underestimated, L/D_{ext} is ~12% underestimated and APB is ~25% underestimated. In any case, it can be underlined that SPREAD tool is able to predict reliable values of APB and L/D_{ext} in a pre-design phase, when a number of configurations have to be analysed, both in fuel-off and fuel-on conditions.

6. Conclusions

The engine and aerothermodynamic modules of SPREAD engineering-based tool have been developed, demonstrated and validated along the LAPCAT-II project, and their accuracy and reliability have been evaluated by comparing results with CFD simulations, available literature results and/or aero-propulsive databases, for a number of significant test cases. The two modules have been then integrated in a common engineering tool for the nose-to-tail analysis of a reference vehicle.
The present paper has described the application of the SPREAD tool to the nose-to-tail analysis of the LAPCAT-II Mach 8 MR2.4 vehicle configuration in hypersonic flight conditions. Both external aerothermodynamics and internal engine’s flowpath have been analysed, and high speed aerodynamic parameters (lift, drag, aerodynamic efficiency) and engine performance parameters (thrust, combustion efficiency, emissions) have been generally well predicted with respect to the CFD results.
It has been demonstrated that SPREAD tool is able to quickly predict reliable values of aero-propulsive balance (i.e., net-thrust) and aerodynamic efficiency, as well as pressure distribution on the external surfaces of the vehicle, when a number of configurations have to be analysed (fuel-off and fuel-on conditions) and CPU-consuming CFD simulations and/or costly experimental test campaigns are not allowed.
However, it must be said that some limitations are still present in the current version of SPREAD code, mainly related to the modelling of combustor: i) calculation of pressure and temperature increases inside the combustor due to the presence of struts (currently taken from CFD), ii) modelling of combustor with a staged injection strategy with multiple struts, and iii) modelling of train of shock waves inside the combustor.

7. Acknowledgements

This work was performed within the ‘Long-Term Advanced Propulsion Concepts and Technologies II’ project investigating high-speed transport. LAPCAT II, coordinated by ESA-ESTEC, is supported by the EU within the 7th Framework Programme Theme7 Transport, Contract no.: ACP7-GA-2008-211485. Further info on LAPCAT II can be found on http://www.esa.int/techresources/lapcat_II.

8. References

[1] Fry, Ronald S., A. 2004. Century of Ramjet Propulsion Technology Evolution. *J. Propul. Power*, 20, (1): 27-58.
[2] Piscitelli, F. 2013. SPREAD: engine design tool development, demonstration and validation. LAPCAT-II project, contract EU-FP7 ACP7-GA-2008-211485, deliverable D4.3.3 and D4.3.6, CIRA-CF-13-0905.
[3] Piscitelli, F., Cutrone, L., Roncioni, P., Natale, P. 2013. SPREAD: an Engineering Tool for Preliminary Design of Hypersonic Airbreathing Vehicles. In: 21st ISABE Conference.
[4] Pezzella, G., Marini, M. 2012. SPREAD design tool: aerothermodynamic module validation. LAPCAT-II project, contract EU-FP7 ACP7-GA-2008-211485, deliverable D4.3.8, CIRA-CF-12-1508.
[5] Roncioni, P., Natale, P., Marini, M., Langener, T., Steelant, J. 2015. Numerical Simulatoins and Perfomance Assessment of a Scramjet Powered Cruise Vehicle at Mach 8. *Aerospace Science and Technology*, 42: 218-228.
[6] Steelant, J. 2009 . Sustained Hypersonic Flight in Europe: Technology Drivers for LAPCAT II. In: 16th AIAA/DLR/DGLR International Space Planes and Hypersonic System Technologies Conference.
[7] Murray N., Steelant J., Mack, A. 2010. Design Evolution for Highly Integrated Hypersonic Vehicles. In: Space Propulsion.
[8] Langener, T., Steelant, J., Roncioni, P., Natale, P., Marini, M., 2012. Preliminary Performance Analysis of the LAPCAT MR2 by means of Nose-to-Tail Computations. In: 18th AIAA International Space Planes and Hypersonic Systems and Technologies Conference.
[9] Roncioni, P., Natale, P., Marini, M., Langener, T., Steelant, J. 2013. Numerical Simulations of the LAPCAT MR-2 Vehicle Scramjet Engine. In: 21st ISABE Conference.
[10] Pezzella, G., Marini, M., Cicala, M., Vitale, A., Langener, T., Steelant, J. 2014. Aerodynamic Characterization of HEXAFLY Scramjet Propelled Hypersonic Vehicle. In: 32nd AIAA Aviation (Applied Aerodynamics Conference).
[11] Bonner, E., Clever, W., Dunn, K. 1991. Aerodynamic Preliminary Analysis System II. Part I-Theory. NASA Contractor Report 182076.
[12] Bertin, J.J. 1994. Hypersonic Aerothermodynamics. AIAA Educational Series, J.S. Przemieniecki editor-in-chief, published by American Institute of Aeronautics and Astronautics, Inc., Washington, DC.
[13] Pezzella, G. 2013. Hypersonic Aerothermal Environment Assessment of the CIRA FTB-X Reentry Vehicle. *Aerospace Science and Technology*, 25, (1): 190-202.
[14] Pezzella, G., Marino, G., Rufolo, G. 2014. Aerodynamic Database Development of the ESA Intermediate Experimental Vehicle. *Acta Astronautica*, 94, (1): 57–72.